Structural Investigation into the Differential Target Enzyme Regulation Displayed by Plant Calmodulin Isoforms†

Aaron P. Yamniuk and Hans J. Vogel*

Structural Biology Research Group, Department of Biological Sciences, University of Calgary, Calgary, AB, Canada T2N 1N4

Received October 19, 2004; Revised Manuscript Received December 10, 2004

ABSTRACT: The conserved calmodulin (CaM) isoform SCaM-1 and the divergent SCaM-4 from soybean bind to many of the same target enzymes, but differentially activate or competitively inhibit them. Class 1 target enzymes are activated by both calcium (Ca^{2+})-bound SCaM-1 (Ca^{2+}-SCaM-1) and Ca^{2+}-bound SCaM-4 (Ca^{2+}-SCaM-4), while class 2 enzymes are activated by Ca^{2+}-SCaM-1 but competitively inhibited by Ca^{2+}-SCaM-4, and class 3 enzymes are activated by Ca^{2+}-SCaM-4 but competitively inhibited by Ca^{2+}-SCaM-1. To determine whether these differences can be attributed to unique interactions with the CaM-binding domains (CaMBD) of these enzymes, we have studied the binding of each protein to peptides derived from the CaMBD of a representative target enzyme from each of these three classes. Using a combination of NMR spectroscopy and isothermal titration calorimetry, we demonstrate that the N- and C-domains of either Ca^{2+}-SCaM bind to each peptide to form structurally compact complexes driven by the burial of hydrophobic surfaces. Interestingly, the interactions with the CaMBD peptides from classes 1 and 2 are similar for the two proteins; however, binding to the peptide from class 3 is structurally and thermodynamically distinct for Ca^{2+}-SCaM-1 and -4. We also demonstrate that both calcium-free SCaM-1 (apo-SCaM-1) and calcium-free SCaM-4 (apo-SCaM-4) bind to the CaMBD from cyclic nucleotide phosphodiesterase, and that the interactions are similar to each other and to the interactions with apo-mammalian CaM. Therefore, the apo-SCaMs are also capable of binding to the same target enzymes, which could provide an additional mechanism for CaM-dependent signaling in plants.

Calmodulin (CaM[1]) is an essential regulatory calcium (Ca^{2+})-binding protein in both animals and plants (*1*, *2*). The X-ray crystal and solution NMR structures of mammalian CaM (mCaM) show it to be a predominantly α-helical protein with distinct N- and C-terminal globular domains connected by a flexible central linker (*3*−*5*). Ca^{2+} binding to mCaM causes interdomain conformational rearrangements, resulting in the exposure of a hydrophobic patch on the surface of each domain. These hydrophobic patches, which are especially rich in Met residues, are the primary surface for interaction with 15−30 amino acid long sequences in target proteins. Studies with synthetic peptides derived from these CaM-binding domains (CaMBDs) have proven to be excellent models for the types of interactions that can occur with intact target enzymes (*6*−*8*). The classical binding mode revealed by these studies involves the N- and C-domains of Ca^{2+}-bound mCaM (Ca^{2+}-mCaM) wrapping around a predominantly α-helical target peptide sequence to form a compact globular structure. However, in recent years several novel modes of binding to target enzymes and CaMBD peptides have been described where Ca^{2+}-mCaM binds in unique compact or even extended conformations (*9*−*12*). There have also been numerous reports describing interactions between Ca^{2+}-free mCaM (apo-mCaM) and various target proteins and peptides (*13*, *14*).

In contrast to the single CaM isoform found in mammals, plants contain numerous different CaM isoforms, many of which have different capacities to activate target enzymes (*15*, *16*). For example, soybean contains five CaM genes (*SCaM1*−*5*), three of which, *SCaM-1*−*3*, code for conserved CaMs with more than 90% sequence identity to mCaM, and two of which, *SCaM-4* and −*5*, code for more divergent isoforms with about 78% sequence identity (*16*). Enzyme activation studies with the SCaM-1 and -4 proteins have indicated that three different classes of target enzymes exist (*17*, *18*). Class 1 enzymes are those that are activated by both Ca^{2+}-bound SCaM-1 (Ca^{2+}-SCaM-1) and Ca^{2+}-bound SCaM-4 (Ca^{2+}-SCaM-4), class 2 enzymes are only activated

† This work was supported by an operating grant from the Natural Sciences and Engineering Research Council of Canada (NSERC). H.J.V. is a Senior Scientist award holder from the Alberta Heritage Foundation for Medical Research (AHFMR), while A.P.Y. holds both AHFMR and NSERC studentship awards. The isothermal titration microcalorimeter was purchased through a grant from the Alberta Science and Research Authority (ASRA) to the Alberta Network of Proteomics Innovation. The Bio-NMR center at the University of Calgary was recently expanded through generous grants from the Canada Foundation for Innovation, ASRA, and AHFMR, and is maintained through funds provided by the Canadian Institutes for Health Research (CIHR) and the University of Calgary.

* To whom correspondence should be addressed. Phone (403) 220-6006. Fax: (403) 289-9311. E-mail: vogel@ucalgary.ca.

[1] Abbreviations: CaM, calmodulin; Ca^{2+}, calcium ion; CaMBD, calmodulin-binding domain; mCaM, mammalian calmodulin; SCaM, soybean calmodulin; NOS, nitric oxide synthase; NMR, nuclear magnetic resonance; ITC, isothermal titration calorimetry; CaMKIIp, calmodulin-dependent protein kinase II peptide; smMLCKp, smooth muscle myosin light-chain kinase peptide; cNOSp, cerebellar nitric oxide synthase peptide; PDEp, cyclic nucleotide phosphodiesterase peptide; HSQC, heteronuclear single-quantum coherence; TEMPOL, 4-hydroxyl-2,2,6,6-tetramethylpiperidinyl-1-oxy; PFG, pulsed field gradient; R_h, hydrodynamic radius; yCaM, yeast calmodulin.

10.1021/bi047770y CCC: $30.25
Published on Web 02/02/2005

by Ca^{2+}-SCaM-1, and class 3 proteins are only activated by Ca^{2+}-SCaM-4. However, for the class 2 and 3 enzymes the SCaM that is incapable of stimulating the activity retains the ability to bind to the enzyme and thus acts as a competitive inhibitor. Studies using mCaM point mutants have shown that SCaM-1's inability to activate the class 3 enzyme nitric oxide synthase (NOS) is due to the M144V point mutation to a predicted CaMBD-coordinating residue (*19*). In contrast the K30E and G40D mutations occur in regions of the SCaM-4 protein that are not directly involved in coordinating the CaMBD, yet they can disrupt its ability to activate some class 2 enzymes (*20*, *21*). Since it remains unclear exactly how binding and activation are affected at the structural level, we have used nuclear magnetic resonance (NMR) spectroscopy and isothermal titration calorimetry (ITC) to study the interactions of Ca^{2+}-SCaM-1 and -4 with peptides derived from the CaMBDs of a representative target enzyme from each of the three classes. Our studies provide both a structural and a thermodynamic description of these interactions with a particular emphasis on the binding interface of each SCaM−peptide complex. Peptides derived from the CaMBD of CaM-dependent protein kinase II (CaMKIIp), smooth muscle myosin light-chain kinase (smMLCKp), and cerebellar NOS (cNOSp) were used as representatives from classes 1−3, respectively. Additionally, since there is relatively little known about the structure or function of Ca^{2+}-free (apo) plant CaM isoforms, we have studied the interactions of apo-SCaM-1 and -4 with the CaMBD peptide from cyclic nucleotide phosphodiesterase (PDEp). This is a well-known apo-mCaM-binding peptide which binds to the C-domain of apo-mCaM, retaining the elongated structure of the protein (*22*, *23*).

MATERIALS AND METHODS

Protein Purification and Peptide Synthesis. A pET-3d expression vector housing either the chimeric SCaM-1 or SCaM-4 genes was cloned into *Escherichia coli* expression strain BL21 DE3, and the unlabeled proteins, [^{13}C]methylmethionine ([^{13}C]Met)-labeled proteins, and mammalian CaM were expressed and purified as described previously (*16*, *24*). Protein concentrations were determined by using the molar extinction coefficients ϵ_{276}(SCaM-1) = 1450 and ϵ_{276}(SCaM-4 = 2900), or by using the Bio-Rad protein assay kit.

The smMLCKp (Ac-ARRKWQKTGHAVRAIGRLSS-NH_2), cNOSp (KRRAIGFKKLAEAVKFSAKLMGQ), CaMKIIp (LKKFNARRKLKGAILTTMLATRNFS-NH_2), and PDEp (Ac-QTEKMWQRLKGILRCLVKQL-NH_2) were each synthesized commercially. Peptide purity was confirmed to be more than 95% by high-pressure liquid chromatography and matrix-assisted laser desorption ionization mass spectrometry. The concentrations of smMLCKp and PDEp were determined using their predicted molar extinction coefficients ϵ_{280} = 5690. Due to the presence of counterions and salts in the lyophilized product, the spectrophotometrically determined concentration of these and nearly all other peptides used in our laboratory are typically ~30% less than what is expected on the basis of the weight of the peptide. Therefore, since cNOSp and CaMKIIp do not contain any Trp or Tyr residues, their concentrations were determined by weighing the lyophilized peptide in a defined volume and multiplying by a correction factor of 0.7.

Nuclear Magnetic Resonance Spectroscopy. All ^{1}H, ^{13}C heteronuclear single-quantum coherence (HSQC) NMR spectra were acquired at 298 K on a Bruker Avance 500 MHz NMR spectrometer equipped with a triple-resonance inverse Cyroprobe with a single-axis *z*-gradient. Studies were performed in 100 mM KCl, 10 mM d_{10}-DTT, 99.9% D_2O, pD 7.5 ± 0.1 (not corrected for isotope effects), and either 4 mM EDTA for apo-SCaM samples or 4 mM $CaCl_2$ for Ca^{2+}-SCaM samples. Titrations with 4-hydroxyl-2,2,6,6-tetramethylpiperidinyl-1-oxy (TEMPOL) (Sigma) were performed using 400 μM samples of [^{13}C]Met-SCaM-1 or -4 titrated with a freshly prepared concentrated stock solution of TEMPOL in 100 mM KCl, 99.9% D_2O, pD 7.5 ± 0.1 (not corrected for isotope effects). For peptide binding studies, samples of 500−600 μM [^{13}C]Met-SCaM-1 or -4 were titrated with concentrated stock solutions of smMLCKp, cNOSp, CaMKIIp, or PDEp, each in the same solution conditions as described above. After each peptide was titrated to 1.1 molar equivalents, each sample was used for pulsed field gradient (PFG) diffusion NMR spectroscopy studies as described below. Then a ^{1}H, ^{13}C HSQC spectrum was rerecorded to ensure sample integrity, and the samples were subsequently each titrated with TEMPOL as done with the peptide-free proteins. All spectra were recorded with a real data spectral size of 2048 × 64 points, sweep widths of 6009.6 and 500 Hz, and carrier frequencies of 500.13235 and 125.7596 MHz for the ^{1}H and ^{13}C dimensions, respectively, with four scans per experiment. Quadrature detection in the F_1 dimension was obtained using echo/antiecho time-proportional phase incrementation. Calculations of solvent-accessible surface area were performed using GetArea 1.1 (*25*).

The PFG diffusion NMR spectra were all acquired on a 700 MHz Bruker shielded magnet equipped with a ^{1}H, X, ^{13}C probe with triple-axis gradients using acquisition and processing parameters similar to those of our previous experiments (*22*), except that 32 transients were acquired at each gradient strength for all samples. Spectra were acquired using the [^{13}C]Met-SCaM−peptide samples described above, as well as with 500 μM samples of peptide-free apo- and Ca^{2+}-[^{13}C]Met-SCaM-1 and -4, or 500 μM samples of unlabeled mCaM.

Isothermal Titration Calorimetry. ITC experiments were performed on a MicroCal VP-ITC microcalorimeter. In each experiment 3−4 μL injections of a concentrated peptide solution were added into a 1.43 mL sample cell containing 12−20 μM SCaM-1 or -4 or mCaM at temperatures ranging from 10 to 30 °C. For studies of Ca^{2+}-dependent peptide binding, lyophilized SCaM-1 or -4 was dissolved in 20 mM HEPES, 100 mM KCl, 10 mM DTT, pH 7.3, and incubated at room temperature overnight to ensure that no SCaM dimers were present through disulfide bonding of Cys26. Immediately prior to ITC analysis, DTT was removed from each SCaM sample by desalting into 20 mM HEPES, 100 mM KCl, pH 7.3, using an Econo-Pac 10DG column (BioRad). These samples were then diluted with the same buffer, and $CaCl_2$ was added to a final concentration of 2 mM using a 1 M stock solution. Since smMLCKp, cNOSp, nor CaMKIIp contains any Cys residues, each peptide was simply dissolved in 20 mM HEPES, 100 mM KCl, 2 mM $CaCl_2$, pH 7.3. For titrations of apo-SCaM-1 or -4 or mCaM with PDEp, lyophilized protein and peptide were each

Table 1: Methionine Residues in CaM Isoforms

	M36	M51	M71	M72	M76	M109	M124	M144	M145	M146
mCaM	√	√	√	√	√	√	√	√	√	
SCaM-1	√	√		√	√	√	√		√	√
SCaM-4		√		√		√	√	√	√	√

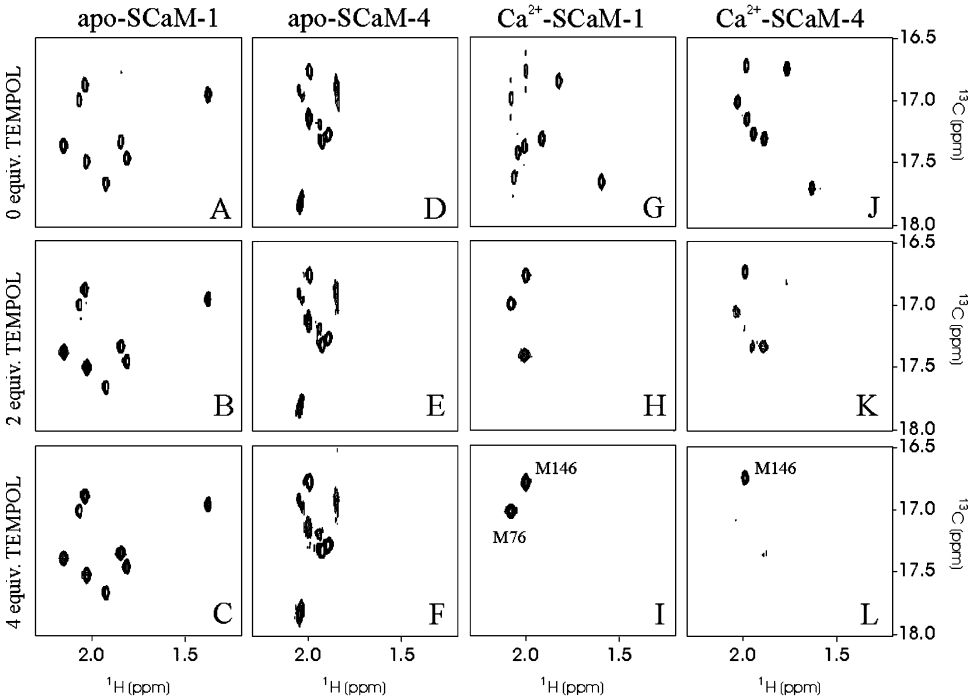

FIGURE 1: ^{1}H, ^{13}C HSQC NMR spectra of apo- and Ca^{2+}-[^{13}C]Met-SCaM-1 or -4 in the presence of 0 (A, D, G, J), 2.0 (B, E, H, K), and 4.0 (C, F, I, L) molar equivalents of TEMPOL.

dissolved in 20 mM HEPES, 100 mM KCl, 1 mM β-mercaptoethanol (βME), pH 7.3, and dialyzed in the same buffer for 3 days at 4 °C. These samples were then diluted with the dialysis buffer, and EDTA was added to both protein and peptide to a final concentration of 2 mM, before the ITC experiments were performed at 25 °C. The heat of dilution/mixing was determined in separate control experiments or by taking the average heat of injection after saturation as is commonly done (*26*), and these values were subtracted in each case. Data were analyzed using MicroCal Origin software to obtain values of stoichiometry (N), association constant (K_a), and enthalpy change (ΔH), while the Gibbs free energy (ΔG), entropy (ΔS), and heat capacity (ΔC_p) changes were calculated using eqs 1 and 2.

$$\Delta G = \Delta H - T\Delta S \quad (1)$$

$$\Delta C_p = \mathrm{d}\Delta H/\mathrm{d}T \quad (2)$$

RESULTS

Solvent Exposure of Hydrophobic Patches. To determine if Ca^{2+} binding to SCaM-1 and -4 causes exposure of Met-rich hydrophobic binding patches similar to those of mCaM, apo- and Ca^{2+}-[^{13}C]Met-SCaM-1 and -4 were titrated with the soluble paramagnetic probe TEMPOL and the effects on the Met methyl resonances were monitored. The paramagnetic nitroxide of TEMPOL is known to increase the relaxation rate of residues that are exposed to the solvent, which broadens their peaks in the NMR spectrum, while buried residues remain unaffected. The highly nonpolar property of TEMPOL makes it an excellent probe for hydrophobic surfaces in proteins, while charged surfaces are less affected. This is best observed with Ca^{2+}-mCaM, where all eight Met's included in the hydrophobic binding patches are very sensitive to TEMPOL-induced broadening, whereas the solvent-exposed M76 in the central linker is unaffected presumably because the neighboring charged side chains repel the very nonpolar TEMPOL molecule (*27*). A similar approach has also been used to study hydrophobic surfaces in several other proteins (*28*, *29*).

The ^{1}H, ^{13}C HSQC spectrum of apo-[^{13}C]Met-SCaM-1 consists of eight well-defined peaks with narrow line widths arising from the eight Met's in the protein, Table 1, Figure 1A. The spectrum of apo-[^{13}C]Met-SCaM-4 consists of approximately seven major peaks from the seven Met's of SCaM-4 in chemical exchange with several minor peaks, indicating that apo-SCaM-4 is either flexible or aggregating or a combination of both, Figure 1D. The spectra of both Ca^{2+}-[^{13}C]Met-SCaM-1 and Ca^{2+}-[^{13}C]Met-SCaM-4 (Figure 1G,J) consist of the expected eight and seven peaks, respectively, which like those of apo-SCaM-1 have line widths characteristic of monomeric globular proteins. The subsequent titrations with TEMPOL induced essentially no peak shifting in any of the spectra, indicating that TEMPOL does not alter the conformation of either protein. Increasing amounts of TEMPOL also did not significantly affect the Met methyl resonances of either apo-[^{13}C]Met-SCaM-1 or apo-[^{13}C]Met-SCaM-4, indicating that the Met's of each apo-SCaM are predominantly shielded from the solvent like those of apo-mCaM, Figure 1B,C,E,F. This result also suggests

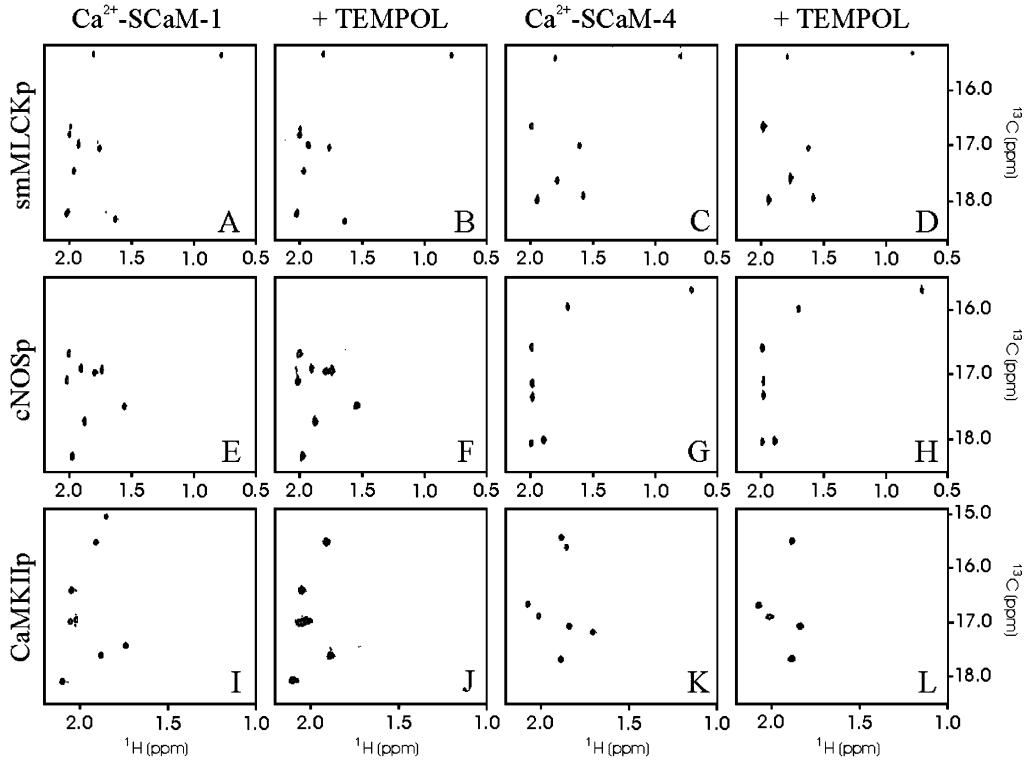

FIGURE 2: ^{1}H, ^{13}C HSQC NMR spectra of Ca^{2+}-[^{13}C]Met-SCaM-1 or -4 in complex with smMLCKp, cNOSp, and CaMKIIp, as well as each complex in the presence of 4.0 molar equivalents of TEMPOL.

that the chemical shift degeneracy and exchange behavior observed with apo-SCaM-4 are more likely due to aggregation than from the protein adopting a flexible partially unfolded conformation, since the latter would in all likelihood involve at least temporary exposure of some Met side chains. Moreover, exposed hydrophobic surfaces were not detected for either apo-SCaM using fluorescence spectroscopy of the hydrophobic fluorescent probe 8-anilino-1-naphthalenesulfonate (ANS) (unpublished observations), confirming that both apoproteins are folded.

In contrast to those of the apo-SCaMs, the majority of Met methyl groups in the Ca^{2+}-bound SCaMs are significantly broadened in the presence of 2 and even more broadened in the presence of 4 molar equivalents of TEMPOL, Figure 1H,I,K,L. This result is consistent with the transition of the Met's from a more buried to a solvent-exposed state upon Ca^{2+} binding. However, two peaks in the Ca^{2+}-SCaM-1 spectrum and 1 peak in the Ca^{2+}-SCaM-4 spectrum were not significantly affected by TEMPOL. One of the Ca^{2+}-SCaM-1 peaks was assigned as M76, since it has a chemical shift nearly identical to that of M76 of Ca^{2+}-mCaM, and like Ca^{2+}-mCaM, Ca^{2+}-SCaM-1 undergoes no Ca^{2+}-induced chemical shift changes (results not shown). The other unaffected peak was predicted to arise from M146 of either protein, which is not found in mCaM and is a residue which faces away from the hydophobic patches surrounded by charged side chains in the crystal structure of the protein (*3*). We confirmed that this peak does correspond to M146 since the peak is missing from a similar HSQC spectrum of a SCaM-4 M146L point mutant (results not shown). Therefore, overall these results suggest that, like that of mCaM, Ca^{2+} binding induces conformational changes which expose Met-rich hydrophobic binding patches on the surface of both SCaM-1 and SCaM-4 which can be probed with TEMPOL.

NMR Studies of Ca^{2+}-SCaM−Peptide Interactions. We have previously demonstrated that since six out of the seven Met's of SCaM-4 are conserved in SCaM-1, we can compare the peptide-bound ^{1}H, ^{13}C HSQC NMR spectra of the [^{13}C]-Met-labeled proteins to determine if the structure at the binding interface and thus overall structure of each SCaM−peptide complex are similar (*24*). Here a similar approach has been used to study the complexes of Ca^{2+}-SCaM-1 or -4 with smMLCKp, cNOSp, and CaMKIIp. Additionally, TEMPOL was added to samples of each Ca^{2+}-SCaM−peptide complex to determine if the exposed Met methyl groups become buried upon peptide binding.

Titration of smMLCKp, cNOSp, or CaMKIIp into samples of Ca^{2+}-[^{13}C]Met-SCaM-1 or -4 caused distinct shifts in all of the Met methyl resonances for both proteins, indicating that both domains are involved in binding to each peptide; compare Figures 1 and 2. During each titration we observed the peaks from the complex in slow chemical exchange with the peaks from the unbound proteins, indicative of a high-affinity interaction, a result confirmed by our subsequent ITC studies. In their complexes with smMLCKp we found very similar chemical shifts for the Met methyl groups of both Ca^{2+}-SCaM-1 and -4, suggesting that the binding interfaces were structurally similar in each Ca^{2+}-SCaM−smMLCKp complex, Figure 2A,C. The addition of TEMPOL had little effect on the peak line widths in either spectrum, indicating that the Met's of each protein become buried and therefore the hydrophobic patches must be involved in binding the peptide, Figure 2B,D.

In contrast to those of smMLCKp, the Met methyl peak chemical shifts for Ca^{2+}-SCaM-1 or -4 bound to cNOSp were considerably different from each other, indicating that the interactions at each binding interface were unique, Figure 2E,G. Nevertheless, TEMPOL again had only very minor

effects on the peak line widths, indicating that the Met residues become buried and thus the hydrophobic patches from both domains are also involved in binding to this peptide, Figure 2F,H. Notably, the most distinctly shifted peaks in the Ca^{2+}-[^{13}C]Met-SCaM-4−cNOSp spectra (^{13}C, ∼15.8 ppm; ^{1}H, ∼0.6 ppm) have chemical shifts nearly identical to those of Met144 of mCaM in complex with cNOSp under similar conditions (*30*), suggesting that they likely also correspond to Met144 of SCaM-4. The large chemical shift change for this Met methyl group indicates that it is in a unique and probably structurally important chemical environment, which is consistent with a Met at this position being essential for activation of the NOS enzyme (*19*).

Because the CaMKII enzyme is activated by both Ca^{2+}-SCaM-1 and Ca^{2+}-SCaM-4, we expected to find similar Met methyl group chemical shifts for each protein in complex with this peptide. As expected, we did observe similar chemical shifts in both spectra, Figure 2I,K. However, we found that the addition of TEMPOL caused the complete broadening of two peaks in each spectrum, demonstrating that two Met's are solvent accessible in each Ca^{2+}-SCaM−CaMKIIp complex and thus that the hydrophobic patches might be partially exposed, Figure 2J,L. These two peaks likely correspond to M51 and either M72 or M145, which have C_ϵ solvent-accessible surface areas of 14.5, 5.8, and 6.2 Å^2, respectively, in the crystal structure of the Ca^{2+}-mCaM−CaMKIIp complex (*31*). This is in contrast to the other two common Met's in the hydrophobic patches, M109 and M124, which are each completely shielded from the solvent in this complex. It is important to note that the two TEMPOL-broadened peaks have very similar chemical shifts in each spectrum, indicating that they likely represent the same two Met's in SCaM-1 and -4, and this emphasizes the structural similarity of the binding interfaces of these two complexes.

Thermodynamic Characterization of Ca^{2+}-SCaM−Peptide Interactions. To determine the thermodynamics of each peptide binding to Ca^{2+}-SCaM-1 or -4, ITC studies were performed. Titrations of smMLCKp into Ca^{2+}-SCaM-1 or -4 each produced a sigmoidal binding curve with a stoichiometry near 1 and affinity near $10^{6-}10^{7}$ M^{-1}, indicating that a high-affinity 1:1 complex was formed with each protein, Figure 3A,B, Table 2. At all temperatures the curves retained a similar sigmoidal shape, and thus, they were each fit to a single-site binding model to obtain the thermodynamic parameters for the interaction. Like the interactions of smMLCKp with Ca^{2+}-mCaM (*32*), binding of smMLCKp to the Ca^{2+}-SCaMs proceeds with large negative changes in both ΔH and $T\Delta S$, indicating that the interactions are driven by favorable enthalpy but are entropically unfavorable. At lower temperatures the interaction becomes less exothermic, resulting in less negative ΔH values and smaller heat signals for binding to each protein. However, the changes in ΔH are offset by equal but opposite changes in $-T\Delta S$ (Figure 4A) such that the Gibbs free energy (ΔG) remains relatively constant over our experimental temperature range. This type of enthalpy−entropy compensation has also been previously observed with the SCaMs (*24*), mCaM (*32*, *33*), and other proteins (*34*) binding to various target molecules. The linearity in the relationships between ΔH or $T\Delta S$ and temperature indicates that the same binding event occurs at each temperature, which allows the ΔC_p for the interaction to be calculated. Importantly the ΔC_p of a binding event is proportional to the change in solvent-accessible hydrophobic surface area from the free to bound state (*35*). For smMLCKp binding to Ca^{2+}-SCaM-1 the ΔC_p is −3.5 kJ/mol K, while for binding to Ca^{2+}-SCaM-4 it is −3.7 kJ/mol K. The negative sign for each ΔC_p indicates that the hydrophobic surface area is buried upon the formation of each complex, while the similarities in the ΔC_p values suggest that a comparable amount of hydrophobic surface area becomes buried in each case. This is pictorially represented in the parallel linear regression of the data for each protein in Figure

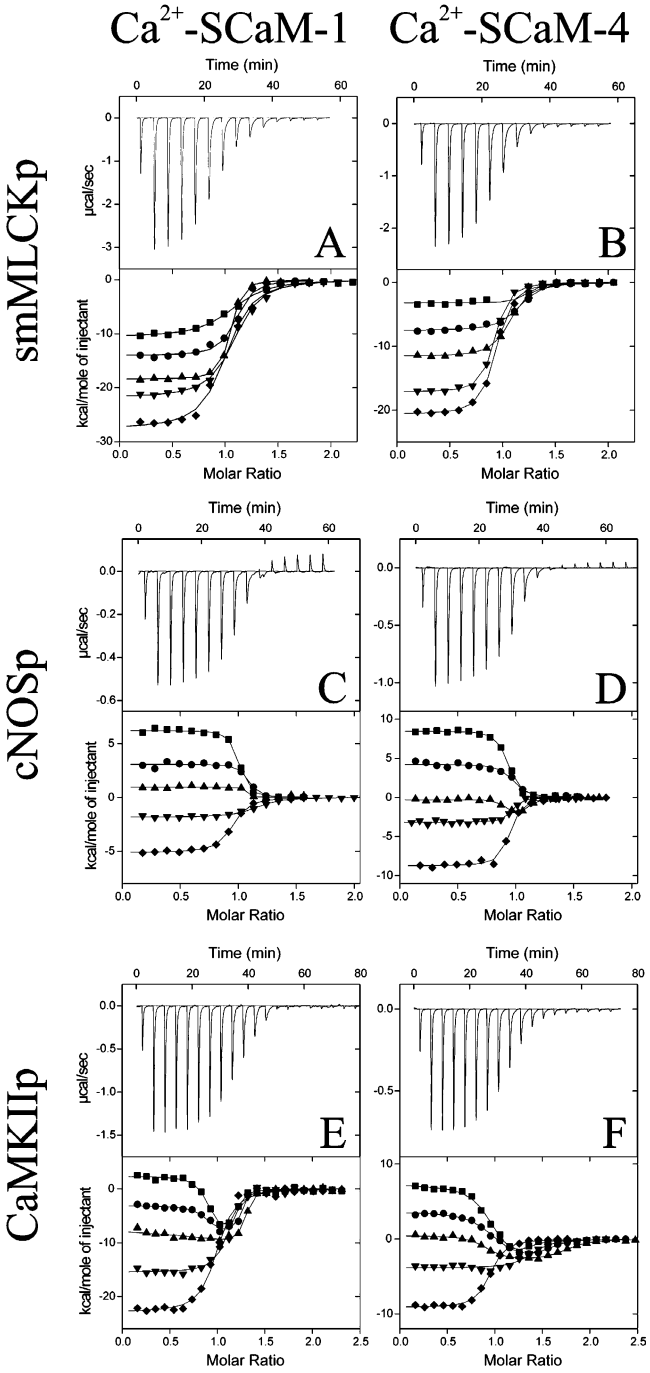

FIGURE 3: Raw calorimetric data for the titration of smMLCKp (A, B), cNOSp (C, D), or CaMKIIp (E, F) into Ca^{2+}-SCaM-1 or -4 at 30 °C (top panels). Derived binding isotherm for each titration performed at 10 °C (■), 15 °C (●), 20 °C (▲), 25 °C (▼), and 30 °C (◆) (bottom panels).

Table 2: Thermodynamics of Ca^{2+}-SCaM−Peptide Interactions Measured by ITC

	temp (°C)	interaction no.	N	K_a (M^{-1})	ΔH (kJ/mol)	$T\Delta S$ (kJ/mol)	ΔG (kJ/mol)
				SCaM-1			
smMLCKp	30		1.0 ± 0.0	(3.9 ± 0.7) × 10^6	−116 ± 2	−77	−38
	25		1.0 ± 0.0	(4.3 ± 0.7) × 10^6	−92 ± 1	−54	−38
	20		1.0 ± 0.0	(3.0 ± 0.4) × 10^7	−77 ± 0	−35	−42
	15		1.1 ± 0.0	(1.1 ± 0.3) × 10^7	−59 ± 1	−20	−39
	10		1.0 ± 0.0	(2.3 ± 0.4) × 10^6	−44 ± 1	−10	−35
cNOSp	30		0.9 ± 0.0	(9.6 ± 0.8) × 10^6	−21 ± 0	19	−41
	25		1.1 ± 0.0	(5.1 ± 1.0) × 10^6	−8 ± 0	31	−38
	20		1.0 ± 0.0		4 ± 0		
	15		1.0 ± 0.0	(3.4 ± 1.7) × 10^7	13 ± 0	54	−42
	10		1.0 ± 0.0	(3.4 ± 0.8) × 10^7	26 ± 0	67	−41
CaMKIIp	30	I	1.0 ± 0.0	(8.5 ± 1.6) × 10^6	−96 ± 1	−55	−40
		II					
	25	I	1.1 ± 0.0	(1.4 ± 0.4) × 10^7	−65 ± 1	−24	−41
		II					
	20	I	1.0 ± 0.1	(6.7 ± 3.7) × 10^7	−30 ± 6	14	−44
		II	0.3 ± 0.6	(3.0 ± 0.0) × 10^7	−68 ± 18	−24	−44
	15	I	0.8 ± 0.0	(1.1 ± 1.0) × 10^9	−13 ± 1	37	−50
		II	0.4 ± 0.0	(2.4 ± 1.1) × 10^7	−36 ± 4	4	−41
	10	I	0.9 ± 0.0	(5.2 ± 3.7) × 10^8	10 ± 1	57	−47
		II	0.3 ± 0.0	(1.1 ± 0.5) × 10^7	−41 ± 7	−3	−38
				SCaM-4			
smMLCKp	30		0.9 ± 0.0	(1.1 ± 0.1) × 10^7	−87 ± 1	−46	−41
	25		0.9 ± 0.0	(1.5 ± 0.1) × 10^7	−72 ± 0	−31	−41
	20		1.0 ± 0.0	(9.1 ± 1.2) × 10^6	−48 ± 0	−9	−39
	15		1.1 ± 0.0	(7.3 ± 1.5) × 10^6	−31 ± 0	6	−38
	10		1.2 ± 0.0	(1.9 ± 1.6) × 10^7	−13 ± 0	26	−39
cNOSp	30		0.9 ± 0.0	(1.9 ± 0.4) × 10^7	−37 ± 0	6	−42
	25		0.9 ± 0.0	(2.8 ± 1.0) × 10^7	−13 ± 0	29	−43
	20		0.9 ± 0.0		−1 ± 0		
	15		0.9 ± 0.0	(1.7 ± 0.8) × 10^7	18 ± 0	58	−40
	10		0.9 ± 0.0	(2.7 ± 0.5) × 10^7	36 ± 0	76	−40
CaMKIIp	30	I	0.9 ± 0.0	(9.6 ± 1.3) × 10^6	−38 ± 0	2	−41
		II					
	25	I	1.4 ± 0.0	(7.2 ± 2.5) × 10^6	−16 ± 0	23	−39
		II					
	20	I	0.9 ± 0.0	(2.2 ± 1.2) × 10^8	2 ± 0	49	−47
		II	0.9 ± 0.0	(3.4 ± 1.1) × 10^6	−12 ± 1	23	−35
	15	I	0.9 ± 0.0	(1.0 ± 0.5) × 10^8	15 ± 0	60	−44
		II	0.6 ± 0.0	(3.9 ± 1.5) × 10^6	−13 ± 2	22	−35
	10	I	0.9 ± 0.0	(6.6 ± 8.5) × 10^7	31 ± 1	73	−42
		II	0.4 ± 0.1	(2.7 ± 2.8) × 10^6	−18 ± 11	17	−34

4A. Therefore, our ITC results are consistent with our NMR data, suggesting that the interactions of both Ca^{2+}-SCaM-1 and Ca^{2+}-SCaM-4 with smMLCKp are highly alike.

Like those of smMLCKp, the binding curves for cNOSp titrated into both Ca^{2+}-SCaM-1 and Ca^{2+}-SCaM-4 were sigmoidal at all temperatures with a stoichiometry near 1, and a comparable affinity, Figure 3C,D. Therefore, these curves were also each fit to a single-site binding model. As seen in Table 2, the ΔH of cNOSp binding to either protein is considerably smaller than with smMLCKp, while the $T\Delta S$ values are positive. This indicates that binding of cNOSp is predominantly driven by favorable entropic factors. Entropy-mediated binding has also been observed for several CaMBD peptides including cNOSp binding to Ca^{2+}-mCaM (*33*). As with smMLCKp, ΔH becomes more positive at lower temperatures, but with cNOSp the interaction actually switches from exothermic at higher temperatures to endothermic at lower temperatures, a result also found with cNOSp binding to Ca^{2+}-mCaM (*33*). Nevertheless, the changes in ΔH and $T\Delta S$ with temperature again offset, giving relatively constant ΔG values, and the linearity in these relationships with respect to temperature allows the ΔC_p to be calculated, Figure 4B. Importantly, the ΔC_p values were considerably different for binding to Ca^{2+}-SCaM-1, −2.3 kJ/mol K, and Ca^{2+}-SCaM-4, −3.5 kJ/mol K, indicating that the structure of the binding interface is different in each complex, consistent with our NMR results. This is also obvious from the nonparallel linear regression of the ΔH and $-T\Delta S$ data for each protein in Figure 4B. The larger ΔC_p for cNOSp binding to Ca^{2+}-SCaM-4 suggests that a more extensive hydrophobic interaction surface is formed in this complex than with Ca^{2+}-SCaM-1, which likely contributes to Ca^{2+}-SCaM-1's inability to activate the cNOS enzyme. We also note that each peptide that we have studied by ITC, except cNOSp, has a larger ΔH of binding to Ca^{2+}-SCaM-1 than Ca^{2+}-SCaM-4 including CATPp (*24*), smMLCKp, and CaMKIIp (see below), emphasizing that fewer interactions are formed between Ca^{2+}-SCaM-1 and cNOSp.

On the basis of our NMR results and previous enzyme activation studies, we expected to find similar thermodynamic behavior for our control peptide CaMKIIp binding to both Ca^{2+}-SCaM-1 and Ca^{2+}-SCaM-4. As expected, at 30 °C the peptide bound to both proteins with a similar affinity and a stoichiometry near 1, and the data were thus fit to a single-site binding model, Figure 3E,F, Table 2. Like that of smMLCKp and cNOSp, the ΔH of binding to both proteins became more positive at lower temperatures; however, unexpectedly, the curves also became distinctly biphasic, indicating that more than one interaction was occurring during the titration of CaMKIIp into either protein, Figure

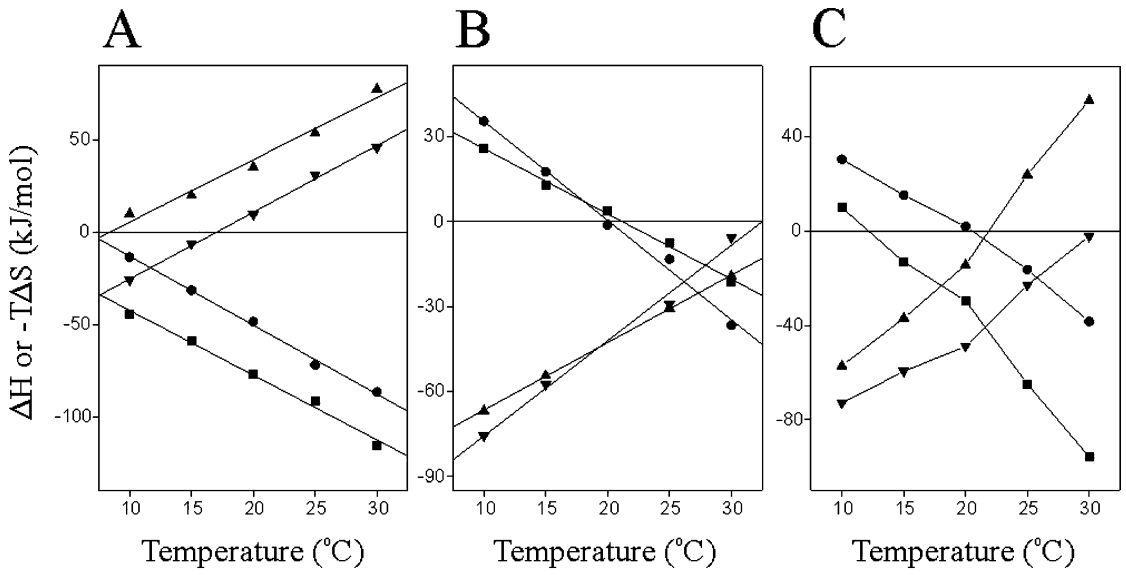

FIGURE 4: Temperature dependence of the enthalpy (ΔH) or entropy ($-T\Delta S$) for Ca^{2+}-SCaM-1 or -4 binding to (A) smMLCKp, (B) cNOSp, and (C) CaMKIIp. In each figure the symbols are as follows: ΔH(Ca^{2+}-SCaM-1−peptide) (■), $-T\Delta S$(Ca^{2+}-SCaM-1−peptide) (▲), ΔH(Ca^{2+}-SCaM-4−peptide) (●), and $-T\Delta S$(Ca^{2+}-SCaM-4−peptide) (▼). The linear regression of the data is shown in (A) and (B), whereas the points in (C) are connected by individual lines (see the text for an explanation). Note that the slope of the ΔH versus temperature curve is equal to the ΔC_p of binding in (A) and (B).

3E,F (bottom panels). At 25 °C the data were still best fit by a single-site binding model; however, at 20, 15, and 10 °C this second binding event was much more evident, and the data for both proteins were best fit to a model which assumed that there were two independent binding events. Although the origin of this second binding event is uncertain, its temperature dependence, exothermic nature, variable low stoichiometry, and appearance late in the titration curve suggest that it is likely due to nonspecific aggregation of the Ca^{2+}-SCaM−CaMKIIp complexes. Furthermore, in other experiments we observed a mild turbidity in solutions of Ca^{2+}-SCaM-1 or -4 upon addition of CaMKIIp near 15−20 °C which disappeared upon warming of the sample to 37 °C (results not shown). Nevertheless, we cannot entirely rule out the possibility that a concentration-dependent conformational rearrangement or some other specific secondary interaction occurs. Whatever the case may be, unfortunately the temperature dependence of binding makes a ΔC_p calculation invalid in the case of CaMKIIp since the best fit values do not represent the same process at each temperature. Therefore, linear regression of the data in Figure 4C was not performed. However, we note that the binding behaviors are qualitatively similar for the two proteins, which is consistent with CaMKII being a class 1 enzyme, capable of being activated by both Ca^{2+}-SCaM-1 and Ca^{2+}-SCaM-4. We also note that although the best fit values defining the curves at 20, 15, and 10 °C are provided in Table 2, they likely do not accurately represent the actual binding mechanism especially if aggregation is the source of the second stage of the curve. Nevertheless, overall the data do show that binding of CaMKIIp to either protein becomes less enthalpically favorable and more entropically favorable at lower temperatures, consistent with the burial of the hydrophobic surface area, which is a common feature of all Ca^{2+}-SCaM− and Ca^{2+}-mCaM−target peptide interactions.

Apo-SCaM−PDEp Interactions. The unique spectral features that we observed for apo-[^{13}C]Met-SCaM-4 motivated our interest in the apo-SCaMs. Therefore, we studied the possible interactions between apo-SCaM-1 or -4 and the well-known apo-mCaM-binding peptide PDEp by both NMR spectroscopy and ITC. Unlike the Ca^{2+}-dependent interactions with smMLCKp, cNOSp, and CaMKIIp, essentially no shifting of any of the Met methyl resonances was observed during titrations of PDEp into either apo-[^{13}C]Met-SCaM-1 or apo-[^{13}C]Met-SCaM-4, Figure 5. Instead some peaks from each spectrum were broadened by chemical exchange, while others were mostly unaffected. This result is consistent with PDEp binding weakly to only one domain of either apo-SCaM. The broadened peaks for apo-SCaM-4 include M146 as identified using the M146L mutant described earlier, indicating that PDEp binds to the C-domain like for apo-mCaM (*23*). It also shows that, despite the tendency for apo-SCaM-4 to aggregate in vitro, the protein retains the ability to bind to PDEp.

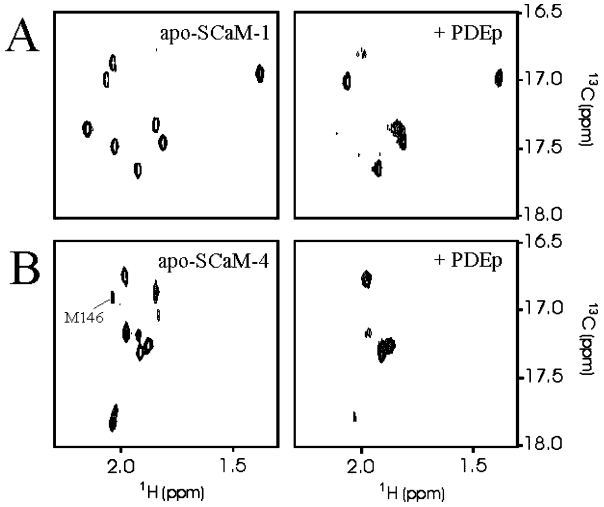

FIGURE 5: ^{1}H, ^{13}C HSQC NMR spectra of (A) apo-[^{13}C]Met-SCaM-1 and (B) apo-[^{13}C]Met-SCaM-4 in the absence and presence of 1.1 molar equivalents of PDEp.

Characterization of the thermodynamics of PDEp binding to apo-SCaM-1 and -4 was performed by ITC at 25 °C.

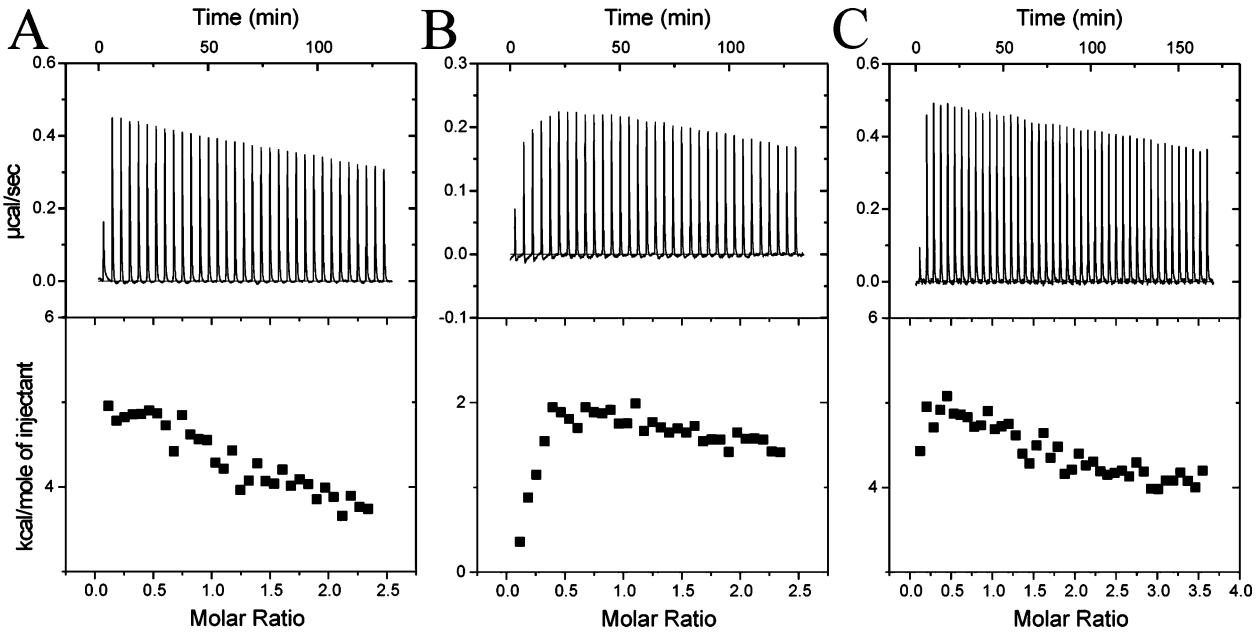

FIGURE 6: Raw ITC calorimetric data (top panels) and derived binding isotherm (bottom panels) for the titration of PDEp into (A) apo-SCaM-1, (B) apo-SCaM-4, and (C) apo-mCaM at 25 °C.

Additionally, the binding of PDEp to apo-mCaM was studied to determine if it was thermodynamically similar to that of the SCaMs. As seen in Figure 6, PDEp binding to each apoprotein produced positive heat signals, indicating that the interactions were endothermic and therefore must be driven by favorable entropy. However, the gradual slope of each binding isotherm indicates that each interaction is relatively weak and is outside the range accurately measured by ITC. Therefore, the data cannot be fit using floating parameters to produce accurate values of N, ΔH, or K_a. Nevertheless, it is possible to make several qualitative conclusions based on these data. For example, the enthalpy of binding to apo-SCaM-4 was considerably lower than that for apo-SCaM-1 or apo-mCaM, which were similar to each other. With apo-SCaM-4 there was also a brief increase in the endothermic signal at the beginning of the titration with a stoichiometry near 0.2, which is likely due to nonspecific interactions or possibly peptide-induced changes in apo-SCaM-4 aggregates. However, the remaining portion of the data for apo-SCaM-4 had a slope similar to those for apo-SCaM-1 and apo-mCaM, suggesting that each interaction was of similar affinity, consistent with homologous interactions between PDEp and apo-SCaM-1 or -4 or -mCaM.

Global Structure of SCaM−Peptide Complexes. To determine if a structural compaction occurs upon Ca^{2+}-SCaM-1 or -4 binding to smMLCKp, cNOSp, and CaMKIIp similar to the interactions of Ca^{2+}-mCaM with these peptides, pulsed field gradient (PFG) diffusion NMR spectroscopy was employed. Additionally, the complexes of mCaM with these peptides were studied under similar conditions, as well as those of the apo-SCaMs and apo-mCaM in the presence and absence of PDEp.

The hydrodynamic radii of each Ca^{2+}-bound protein were similar to the value reported previously for Ca^{2+}-mCaM using small angle X-ray scattering (*36*), which is consistent with elongated dumbbell-shaped structures, Table 3. However, a decrease in R_h was observed for each protein bound to each peptide, indicative of a structural collapse similar to that observed in the crystal structures of Ca^{2+}-mCaM bound to smMLCKp, CaMKIIp, and the cNOSp homologue eNOS peptide (*31*, *37*, *38*). This collapse includes the Ca^{2+}-SCaM-1−cNOSp complex, indicating that the overall mode of binding is retained despite the dissimilar interactions at the protein−peptide interface.

Table 3: Hydrodynamic Radii (R_h) (Å) for SCaM-1− and SCaM-4−Target Peptide Complexes Determined by PFG Diffusion NMR Spectroscopy

		SCaM-1	SCaM-4	mCaM
no peptide	Ca^{2+}	23.3 ± 1.6	23.6 ± 1.6	22.1 ± 1.0
smMLCKp	Ca^{2+}	19.4 ± 0.9	18.2 ± 1.0	19.2 ± 0.6
cNOSp	Ca^{2+}	21.3 ± 1.5	21.0 ± 1.4	18.7 ± 2.0
CaMKIIp	Ca^{2+}	20.2 ± 0.7	17.4 ± 1.5	19.5 ± 1.9
no peptide	apo	22.0 ± 1.3	28.0 ± 1.3	20.3 ± 1.1
PDEp	apo	25.1 ± 3.9	29.7 ± 5.9	22.6 ± 2.7

The average R_h values for apo-mCaM as well as apo-SCaM-1 were moderately smaller than those of the Ca^{2+}-loaded proteins, a result which has also been observed with mCaM using other techniques (*36*, *39*). However, the R_h for apo-SCaM-4 was significantly larger (28.0 ± 1.3 Å), confirming that apo-SCaM-4 aggregates under these conditions. When PDEp was present at stoichiometric amounts in the samples of each apoprotein, the R_h increased by ∼2−3 Å, consistent with binding to only one domain to form a slightly more elongated structure, Table 3. Importantly, the error estimates also increased considerably for the apo-SCaM−PDEp complexes likely because the low-affinity interactions are accompanied by fast on and off rates. Furthermore, the R_h increase observed with apo-SCaM-4 indicates that the aggregates do not completely dissociate upon PDEp binding.

DISCUSSION

In this study we have used both NMR spectroscopy and ITC to test the possibility that the differential enzymatic regulation of target enzymes demonstrated by Ca^{2+}-SCaM-1 and -4 is due to different interactions with the CaMBDs of these enzymes. Like that of mCaM, we have demonstrated

that Ca^{2+} binding to the apo-SCaMs acts as a conformational switch which results in the exposure of a Met-rich hydrophobic binding patch on the surface of both domains that are involved in target peptide interactions. In particular, the Met residues of these hydrophobic binding patches are directly involved in coordinating the peptides smMLCKp, cNOSp, and CaMKIIp, and most of these Mets become shielded from solvent by the interaction. The overall mode of binding is similar to the canonical Ca^{2+}-mCaM−peptide binding mode where both domains of the Ca^{2+}-SCaMs collapse around each target peptide to form a compact globular structure. ITC studies also demonstrated that both Ca^{2+}-SCaM-1 and Ca^{2+}-SCaM-4 bind to each peptide with similar affinity in the range of 10^6-10^7 M^{-1}, suggesting that they could compete for target enzymes if coexpressed in vivo. However, there has as yet been no evidence to suggest that SCaM-1 and -4 are coexpressed in the same cells, and we note that their affinities for the intact target enzymes could actually differ from those of the isolated CaMBDs.

During the course of our studies on SCaM−peptide interactions it became obvious that, despite their sequence divergence, both SCaM-1 and -4 seem to be structurally very similar to mCaM. Although this is important, it should not be very surprising since even CaM from the yeast *Saccharomyces cerevisiae* (yCaM), which has only ~60% sequence identity to mCaM, also adopts a similar secondary structure arrangement consisting of two pairs of helix−loop−helix motifs connected by a central linker (*40*). Our PFG diffusion results show that both Ca^{2+}-SCaMs are extended in solution like Ca^{2+}-mCaM, but unlike Ca^{2+}-yCaM, which adopts a collapsed structure likely due to interactions between the hydrophobic patches of the N- and C-domains (*41*, *42*). This is important to point out because the interaction between the two domains of Ca^{2+}-yCaM is suggested to be responsible for the reduced ability of the protein to activate some target enzymes (*41*, *43*, *44*). Our TEMPOL titrations also suggested that the Met residues of each Ca^{2+}-bound SCaM were exposed to solvent and not buried as would be expected if the two hydrophobic patches were interacting with each other.

Like the interactions of Ca^{2+}-SCaM-1 and -4 with CATPp, our results showed that both proteins bind to either CaMKIIp or smMLCKp in a structurally similar manner. For CaMKIIp this was expected since both proteins can activate the enzyme equally well. However, for smMLCKp this result is important because it confirms that the inability of Ca^{2+}-SCaM-4 to activate the smMLCK enzyme is not due to dissimilar interactions with its CaMBD. Instead, our results support the finding that the K30E and G40D point mutations in predicted non-CaMBD-coordinating residues in the first EF-hand of SCaM-4 are responsible for its failure to activate smMLCK (*21*). On the basis of the structure of Ca^{2+}-mCaM bound to smMLCKp, it was proposed that these two residues face away from the CaMBD, forming a surface which could potentially interact with distal regions of the smMLCK enzyme. Interestingly, these same two point mutations are also responsible for Ca^{2+}-SCaM-4's inability to activate NAD kinase (*20*), suggesting that similar interactions might be a common requirement for activation of several CaM-regulated protein kinases. However, it remains to be determined whether similar mutations contribute to the failure of Ca^{2+}-SCaM-4 to activate other non-kinase enzymes such as calcineurin or erythrocyte Ca^{2+}-ATPase.

In contrast to that of the other peptides, our data demonstrate that the structural recognition of cNOSp is distinct for Ca^{2+}-SCaM-1 and -4. Although each structure is collapsed with a similar binding mode involving interaction of the Met residues from each domain with the peptide, the chemical environments of the Met residues of each protein are different, suggesting that there are unique packing interactions between the side chains of either protein and cNOSp. The smaller ΔC_p and ΔH of cNOSp binding to Ca^{2+}-SCaM-1 suggests that the interface between Ca^{2+}-SCaM-1 and cNOSp is also less extensive and involves fewer hydrophobic interactions. Taken together with the results of Johnson and co-workers (*19*), it seems likely that the shorter Val144 side chain alters the interaction of Ca^{2+}-SCaM-1 with the CaMBD of cNOS, and this results in an inability to activate the enzyme. The fact that the M144V mutation does not affect binding or activation of other enzymes emphasizes the plasticity of CaM's hydrophobic binding patches. Notably, several other plant species contain a CaM isoform with a M144V mutation including carrot, rice, pea, wheat, and apple, among others, suggesting that it might have a common function in many plant species. However, to our knowledge the activation of plant-specific NOS enzymes by SCaM-1 and -4 has not yet been studied, and we note that the only NOS isoform currently identified in plants has little sequence homology to animal NOS enzymes (*45*).

Another possible mechanism that could allow for differential target enzyme regulation by plant CaM isoforms is through interactions with the apoproteins. To our knowledge this possibility has not yet been investigated, yet one study used gel overlay assays to show that both apo-SCaM-1 and apo-SCaM-4 do bind to some proteins in the presence of Ca^{2+} chelators (*17*). Many proteins require apo-mCaM for enzymatic activity, while others have been implicated in CaM storage, and recently even shown to regulate the affinity of CaM for Ca^{2+} (*46*). Our results demonstrate that PDEp binds to the C-domain of both apo-SCaM-1 and apo-SCaM-4, with affinity similar to that of its interactions with apo-mCaM. Binding was also entropically driven, similar to some apo-mCaM−peptide interactions (*47*, *48*), and the R_h of each complex increased in comparison to those of the free apoproteins, consistent with an interaction with only one domain. Therefore, apo-SCaM-1 and -4 also have the potential to bind to the same target enzymes, which could provide an additional regulatory mechanism for CaM-dependent signaling in plants.

ACKNOWLEDGMENT

We express our gratitude to Dr. D. D. McIntyre for continuous upkeep of the NMR instrumentation.

REFERENCES

1. Chin, D., and Means, A. R. (2000) Calmodulin: a prototypical calcium sensor, *Trends Cell Biol. 10*, 322−328.
2. Snedden, W. A., and Fromm, H. (2001) Calmodulin as a versatile calcium signal transducer in plants, *New Phytol. 151*, 35−66.
3. Babu, Y. S., Sack, J. S., Greenhough, T. J., Bugg, C. E., Means, A. R., and Cook, W. J. (1985) Three-dimensional structure of calmodulin, *Nature 315*, 37−40.

4. Kuboniwa, H., Tjandra, N., Grzesiek, S., Ren, H., Klee, C. B., and Bax, A. (1995) Solution structure of calcium-free calmodulin, *Nat. Struct. Biol. 2*, 768−776.
5. Zhang, M., Tanaka, T., and Ikura, M. (1995) Calcium-induced conformational transition revealed by the solution structure of apo calmodulin, *Nat. Struct. Biol. 2*, 758−767.
6. Chin, D., Sloan, D. J., Quiocho, F. A., and Means, A. R. (1997) Functional consequences of truncating amino acid side chains located at a calmodulin-peptide interface, *J. Biol. Chem. 272*, 5510−5513.
7. Gomes, A. V., Barnes, J. A., and Vogel, H. J. (2000) Spectroscopic characterization of the interaction between calmodulin- dependent protein kinase I and calmodulin, *Arch. Biochem. Biophys. 379*, 28−36.
8. Kranz, J. K., Lee, E. K., Nairn, A. C., and Wand, A. J. (2002) A direct test of the reductionist approach to structural studies of calmodulin activity: relevance of peptide models of target proteins, *J. Biol. Chem. 277*, 16351−16354.
9. Hoeflich, K. P. and Ikura, M. (2002) Calmodulin in action: diversity in target recognition and activation mechanisms, *Cell 108*, 739−742.
10. Ishida, H. and Vogel, H. J. (2005) Protein-peptide interaction studies demonstrate the versatility of calmodulin target protein binding, *Protein Pept. Lett*. (in press).
11. Vetter, S. W., and Leclerc, E. (2003) Novel aspects of calmodulin target recognition and activation, *Eur. J. Biochem. 270*, 404−414.
12. Yamniuk, A. P., and Vogel, H. J. (2004) Calmodulin's flexibility allows for promiscuity in its interactions with target proteins and peptides, *Mol. Biotechnol. 27*, 33−57.
13. Bahler, M., and Rhoads, A. (2002) Calmodulin signaling via the IQ motif, *FEBS Lett. 513*, 107−113.
14. Jurado, L. A., Chockalingam, P. S., and Jarrett, H. W. (1999) Apocalmodulin, *Physiol. Rev. 79*, 661−682.
15. Cho, M. J., Vaghy, P. L., Kondo, R., Lee, S. H., Davis, J. P., Rehl, R., Heo, W. D., and Johnson, J. D. (1998) Reciprocal regulation of mammalian nitric oxide synthase and calcineurin by plant calmodulin isoforms, *Biochemistry 37*, 15593−15597.
16. Lee, S. H., Kim, J. C., Lee, M. S., Heo, W. D., Seo, H. Y., Yoon, H. W., Hong, J. C., Lee, S. Y., Bahk, J. D., Hwang, I., and Cho, M. J. (1995) Identification of a novel divergent calmodulin isoform from soybean which has differential ability to activate calmodulin-dependent enzymes, *J. Biol. Chem. 270*, 21806−21812.
17. Lee, S. H., Kim, M. C., Heo, W. D., Kim, J. C., Chung, W. S., Park, C. Y., Park, H. C., Cheong, Y. H., Kim, C. Y., Lee, K. J., Bahk, J. D., Lee, S. Y., and Cho, M. J. (1999) Competitive binding of calmodulin isoforms to calmodulin-binding proteins: implication for the function of calmodulin isoforms in plants, *Biochim. Biophys. Acta 1433*, 56−67.
18. Lee, S. H., Johnson, J. D., Walsh, M. P., Van Lierop, J. E., Sutherland, C., Xu, A., Snedden, W. A., Kosk-Kosicka, D., Fromm, H., Narayanan, N., and Cho, M. J. (2000) Differential regulation of Ca^{2+}/calmodulin-dependent enzymes by plant calmodulin isoforms and free Ca^{2+} concentration, *Biochem. J. 350 Pt 1*, 299−306.
19. Kondo, R., Tikunova, S. B., Cho, M. J., and Johnson, J. D. (1999) A point mutation in a plant calmodulin is responsible for its inhibition of nitric-oxide synthase, *J. Biol. Chem. 274*, 36213−36218.
20. Lee, S. H., Seo, H. Y., Kim, J. C., Heo, W. D., Chung, W. S., Lee, K. J., Kim, M. C., Cheong, Y. H., Choi, J. Y., Lim, C. O., and Cho, M. J. (1997) Differential activation of NAD kinase by plant calmodulin isoforms. The critical role of domain I, *J. Biol. Chem. 272*, 9252−9259.
21. Van Lierop, J. E., Wilson, D. P., Davis, J. P., Tikunova, S., Sutherland, C., Walsh, M. P., and Johnson, J. D. (2002) Activation of smooth muscle myosin light chain kinase by calmodulin. Role of LYS(30) and GLY(40), *J. Biol. Chem. 277*, 6550−6558.
22. Weljie, A. M., Yamniuk, A. P., Yoshino, H., Izumi, Y., and Vogel, H. J. (2003) Protein conformational changes studied by diffusion NMR spectroscopy: application to helix-loop-helix calcium binding proteins, *Protein Sci. 12*, 228−236.
23. Yuan, T., Walsh, M. P., Sutherland, C., Fabian, H., and Vogel, H. J. (1999) Calcium-dependent and -independent interactions of the calmodulin- binding domain of cyclic nucleotide phosphodiesterase with calmodulin, *Biochemistry 38*, 1446−1455.
24. Yamniuk, A. P., and Vogel, H. J. (2004) Structurally homologous binding of plant calmodulin isoforms to the calmodulin-binding domain of vacuolar calcium-ATPase, *J. Biol. Chem. 279*, 7698−7707.
25. Fraczkiewicz, R., and Braun, W. (1998) Exact and efficient analytical calculation of the accessible surface areas and their gradients for macromolecules, *J. Comput. Chem. 19*, 319−333.
26. Pierce, M. M., Raman, C. S., and Nall, B. T. (1999) Isothermal titration calorimetry of protein-protein interactions, *Methods 19*, 213−221.
27. Yuan, T., Ouyang, H., and Vogel, H. J. (1999) Surface exposure of the methionine side chains of calmodulin in solution. A nitroxide spin label and two-dimensional NMR study, *J. Biol. Chem. 274*, 8411−8420.
28. Petros, A. M., Mueller, L., and Kopple, K. D. (1990) NMR identification of protein surfaces using paramagnetic probes, *Biochemistry 29*, 10041−10048.
29. Petros, A. M. and Fesik, S. W. (1994) Nuclear magnetic resonance methods for studying protein-ligand complexes, *Methods Enzymol. 239*, 717−739.
30. Zhang, M., Yuan, T., Aramini, J. M., and Vogel, H. J. (1995) Interaction of calmodulin with its binding domain of rat cerebellar nitric oxide synthase. A multinuclear NMR study, *J. Biol. Chem. 270*, 20901−20907.
31. Meador, W. E., Means, A. R., and Quiocho, F. A. (1993) Modulation of calmodulin plasticity in molecular recognition on the basis of x-ray structures, *Science 262*, 1718−1721.
32. Wintrode, P. L., and Privalov, P. L. (1997) Energetics of target peptide recognition by calmodulin: a calorimetric study, *J. Mol. Biol. 266*, 1050−1062.
33. Brokx, R. D., Lopez, M. M., Vogel, H. J., and Makhatadze, G. I. (2001) Energetics of target peptide binding by calmodulin reveals different modes of binding, *J. Biol. Chem. 276*, 14083−14091.
34. Eftink, M. R., Anusiem, A. C., and Biltonen, R. L. (1983) Enthalpy-entropy compensation and heat capacity changes for protein-ligand interactions: general thermodynamic models and data for the binding of nucleotides to ribonuclease A, *Biochemistry 22*, 3884−3896.
35. Loladze, V. V., Ermolenko, D. N., and Makhatadze, G. I. (2001) Heat capacity changes upon burial of polar and nonpolar groups in proteins, *Protein Sci. 10*, 1343−1352.
36. Seaton, B. A., Head, J. F., Engelman, D. M., and Richards, F. M. (1985) Calcium-induced increase in the radius of gyration and maximum dimension of calmodulin measured by small-angle X-ray scattering, *Biochemistry 24*, 6740−6743.
37. Aoyagi, M., Arvai, A. S., Tainer, J. A., and Getzoff, E. D. (2003) Structural basis for endothelial nitric oxide synthase binding to calmodulin, *EMBO J. 22*, 766−775.
38. Meador, W. E., Means, A. R., and Quiocho, F. A. (1992) Target enzyme recognition by calmodulin: 2.4 A structure of a calmodulin-peptide complex, *Science 257*, 1251−1255.
39. Papish, A. L., Tari, L. W., and Vogel, H. J. (2002) Dynamic light scattering study of calmodulin-target peptide complexes, *Biophys. J. 83*, 1455−1464.
40. Ishida, H., Nakashima, K., Kumaki, Y., Nakata, M., Hikichi, K., and Yazawa, M. (2002) The solution structure of apocalmodulin from Saccharomyces cerevisiae implies a mechanism for its unique Ca^{2+} binding property, *Biochemistry 41*, 15536−15542.
41. Lee, S. Y., and Klevit, R. E. (2000) The whole is not the simple sum of its parts in calmodulin from S. cerevisiae, *Biochemistry 39*, 4225−4230.
42. Yoshino, H., Izumi, Y., Sakai, K., Takezawa, H., Matsuura, I., Maekawa, H., and Yazawa, M. (1996) Solution X-ray scattering data show structural differences between yeast and vertebrate calmodulin: implications for structure/function, *Biochemistry 35*, 2388−2393.
43. Matsuura, I., Kimura, E., Tai, K., and Yazawa, M. (1993) Mutagenesis of the fourth calcium-binding domain of yeast calmodulin, *J. Biol. Chem. 268*, 13267−13273.
44. Ohya, Y., Uno, I., Ishikawa, T., and Anraku, Y. (1987) Purification and biochemical properties of calmodulin from Saccharomyces cerevisiae, *Eur. J. Biochem. 168*, 13−19.
45. Chandok, M. R., Ytterberg, A. J., van Wijk, K. J., and Klessig, D. F. (2003) The pathogen-inducible nitric oxide synthase (iNOS) in plants is a variant of the P protein of the glycine decarboxylase complex, *Cell 113*, 469−482.
46. Gaertner, T. R., Putkey, J. A., and Waxham, M. N. (2004) RC3/Neurogranin and Ca^{2+}/calmodulin-dependent protein kinase II

produce opposing effects on the affinity of calmodulin for calcium, *J. Biol. Chem. 279*, 39374−39382.

47. Censarek, P., Beyermann, M., and Koch, K. W. (2002) Target recognition of apocalmodulin by nitric oxide synthase I peptides, *Biochemistry 41*, 8598−8604.

48. Censarek, P., Beyermann, M., and Koch, K. W. (2004) Thermodynamics of apocalmodulin and nitric oxide synthase II peptide interaction, *FEBS Lett. 577*, 465−468.

BI047770Y